

1     **Anthropogenic footprint of climate change in the June 2013 northern India flood**  
2

3     Changrae Cho<sup>1</sup>, Rong Li<sup>1,2</sup>, S.-Y. (Simon) Wang<sup>1,2</sup>, Jin-Ho Yoon<sup>3</sup>, Robert R. Gillies<sup>1,2</sup>

4             (1) Utah Climate Center, Utah State University, Logan, UT, USA

5             (2) Department of Plants, Soils, and Climate, Utah State University, Logan, UT, USA

6             (3) Pacific Northwest National Laboratory, Richland, Washington

7  
8     Corresponding to: [simon.wang@usu.edu](mailto:simon.wang@usu.edu)

9  
10    Running head: Anthropogenic impact on June 2013 Indian flood  
11

12  
13    **Abstract**

14            During 13-17 June 2013, heavy rainfall occurred in the northern Indian state of  
15    Uttarakhand and led to one of the worst floods in history and massive landslides,  
16    resulting in more than 5,000 casualties and a huge loss of property. In this study,  
17    meteorological and climatic conditions leading up to this rainfall event in 2013 and  
18    similar cases were analyzed for the period of 1979-2012. Attribution analysis was  
19    performed to identify the natural and anthropogenic influences on the climate anomalies  
20    using the historical single-forcing experiments in the Coupled Model Intercomparison  
21    Project Phase 5 (CMIP5). In addition, regional modeling experiments were carried out to  
22    quantify the role of the long-term climate trends in affecting the rainfall magnitude of the  
23    June 2013 event. It was found that (a) northern India has experienced increasingly large  
24    rainfall in June since the late 1980s, (b) the increase in rainfall appears to be associated  
25    with a tendency in the upper troposphere towards amplified short waves, and (c) the  
26    phasing of such amplified short waves is tied with increased green-house gases (GHGs)  
27    and aerosols. In addition, a regional modeling diagnosis attributed 60-90% of rainfall  
28    amounts in the June 2013 event to post-1980 climate trends.

29

30 **Keywords:** Extreme events, climate and weather interactions, greenhouse gas  
31 (GHG) forcing, synoptic wave train, CMIP5, WRF model, cold air intrusion

32

### 33 **1. Introduction**

34         During 13-17 June 2013, heavy rainfall occurred in the northern Indian state of  
35 Uttarakhand, located on the windward side of the Himalayan ranges. The torrential rain  
36 together with rapid snowmelt led to extreme flooding and widespread landslides, causing  
37 thousands of deaths and a huge loss of property (Dubey et al. 2013). In addition to the  
38 devastation in Uttarakhand, this event also affected other parts of India including  
39 Himachal Pradesh, Haryana, Delhi and Uttar Pradesh, as well as western Nepal and parts  
40 of Tibet (Dubey et al. 2013). In recent years, similar heavy rainfall and widespread flood  
41 events have become increasingly frequent in northern South Asia. For example, an  
42 extreme rainfall event occurred in northern Pakistan during July 2010, resulting in floods  
43 that killed about 3,000 and affected around 20 million people (Hong et al. 2011; Lau and  
44 Kim 2012; Wang et al. 2011b). More recently (2-6 September 2014), some regions in  
45 India (Jammu and Kashmir) and Pakistan (Azad Kashmir, Gilgit-Baltistan and Punjab)  
46 underwent extreme floods caused by heavy rainfall, leading to more than 500 deaths  
47 (Najar and Masood, 2014).

48         A number of recent studies have investigated these heavy rainfall events, but most  
49 studies focused on either the synoptic or the mesoscale meteorological conditions of  
50 individual events (e.g., Hong et al. 2011; Houze et al. 2011; Joseph et al. 2014; Martius et  
51 al. 2013); few studies have analyzed the large-scale features and long-term climate

52 linkages. A recent study (Singh et al. 2014) conducted statistical analysis and concluded  
53 that the June 2013 rainstorm in northern India was at least a century-scale event, and the  
54 probability for such an event to occur has increased in the present climate compared to  
55 the preindustrial climate. However, knowledge regarding the mechanisms leading to the  
56 reported increased probability in extreme rainfall is lacking. Isolating the climate change  
57 impact on any individual storm or rainfall event is challenging, but such information is  
58 necessary for disaster planning and mitigation. Thus, the goals of this study are to  
59 identify common features in the meteorological conditions accompanying the June 2013  
60 event and to investigate the mechanism through which climate change influences similar  
61 rainfall events, using observational data and climate model simulations. The data and  
62 modeling system used in this research are described in Section 2. The results are  
63 presented in Section 3. A summary and discussions are provided in Section 4.

64

## 65 **2. Data and Methods**

### 66 **2.1 Data**

67 To depict evolution of the heavy rainfall cases, observational rainfall was obtained  
68 from the 3-hourly Climate Prediction Center (CPC) Morphing technique precipitation  
69 (CMORPH) (Joyce et al. 2004) with the resolution of  $0.25^\circ \times 0.25^\circ$ . Since the CMORPH  
70 exists only after December 2002, monthly global precipitation data from NOAA's  
71 Precipitation Reconstruction over Land (PREC/L) (Chen et al. 2002) for the period of  
72 1948–present was used to analyze the long-term climatology and trend. The PREC/L  
73 dataset is based on the gauge observations over 17,000 stations worldwide, and the  
74 resolution used in this study is  $1.0^\circ \times 1.0^\circ$ . For meteorological variables including wind,

75 temperature, relative humidity, and geopotential height, the NCEP/NCAR Reanalysis  
76 (Kalnay et al. 1996) for the period 1948–present was used.

77 To perform detection and attribution analyses, we used the fully coupled climate  
78 model simulations in the Coupled Model Intercomparison Project Phase 5 (CMIP5)  
79 (Taylor et al. 2012). To isolate the climate change signal, four sets of the CMIP5  
80 Historical Single-Forcing Experiments were used: (a) one driven solely by natural forcing  
81 (e.g., solar cycle and volcano) (denoted as NAT), (b) one forced solely by greenhouse  
82 gases (denoted as GHG), (c) one driven solely by aerosols forcing (denoted as Aero), and  
83 (d) one driven with all natural and anthropogenic forcing sources (Taylor et al. 2012). A  
84 total of 10 coupled models were used in this study, and the details of these models are  
85 listed in Table 1.

86

## 87 **2.2 Regional climate model experiments**

88 Simulations of the June 2013 Indian rainfall event were carried out using the  
89 Weather Research and Forecasting (WRF) model version 3.5 ([http://www.wrf-  
90 model.org/index.php](http://www.wrf-model.org/index.php)). Initial and lateral boundary conditions were obtained from the  
91 NCEP-DOE Reanalysis2 (Kanamitsu et al. 2002), which is 6-hourly data with a  
92 resolution of  $2.5^\circ \times 2.5^\circ$ . WRF simulations were conducted for the period of 1-21 June  
93 2013 and the first 11 days were treated as spin-up. The model land use was derived from  
94 the United States Geological Survey (USGS) 24-category global 30-second dataset. The  
95 spatial resolution was set to 30 km, and the simulations used 30 vertical layers up to 50  
96 mb. The physics parameterizations included the SBU-YLin scheme for microphysics (Lin  
97 and Colle 2011), CAM schemes for radiation (Collins et al. 2006), MYNN level 2.5

98 TKE scheme for the Planetary Boundary Layer (PBL) processes (Nakanishi and Niino  
99 2006), and five-layer soil thermal diffusion scheme for land surface processes.

100 To isolate the effects of climate change on the June 2013 Indian rainfall event,  
101 two experiments were designed:

102 (1) *Control simulation* forced by the initial and boundary conditions (BC) from the  
103 original NCEP-R2 data;

104 (2) *No-trend simulation* forced by the BC of the NCEP-R2 from which the post-1980  
105 linear climate trends in all BC variables were removed. The assumption here is that  
106 any long-term trend manifest in the troposphere contains signals that are traceable to  
107 anthropogenic climate warming (which is supported by CMIP5 attribution analysis as  
108 shown later). Although the long-term changes exhibited by different variables may  
109 not be linearly correlated, we have shown in a previous study (Wang et al. 2011a) that  
110 the nonlinear effect is generally negligible when it comes to this no-trend simulation  
111 approach in South Asia.

112

### 113 **3. Results**

#### 114 **3.1 The heavy rainfall event in June 2013**

115 To depict the large-scale environment associated with the June 2013 flood event,  
116 we divided the evolution of the rainfall event (8-22 June 2013) into three periods: pre-  
117 storm (8-12 June), storm (13-17), and post-storm (18-22) periods. In doing so, we  
118 focused on the large-scale environment and its evolution. Figures 1a and b show the 5-  
119 day averages of wind and vorticity fields during the pre-storm period at 200mb and  
120 700mb, respectively. An upper-level ridge covered most of northern India (Figure 1a),

121 while the monsoon trough center (Figure 1b) was located on the western coast of the  
122 Indian peninsula and the Arabian Sea. Meanwhile a monsoon depression developed over  
123 the Bay of Bengal (BoB) as seen in the lower troposphere. These circulation patterns  
124 changed considerably during the storm period (Figures 1c and d): First, an upper-level  
125 tropospheric trough developed over northern India and appeared to be part of a short-  
126 wave train extending from the Mediterranean Sea to East Asia (Figure 1c). As indicated  
127 by Joseph et al. (2014), this trough over northern India induced cold air intrusion in the  
128 upper troposphere and subsequently enhanced instability in the region. In the lower  
129 troposphere, the BoB depression moved into the Indian subcontinent and merged with the  
130 monsoon trough, forming a strong cyclonic circulation over central and northern India.  
131 The northern branch of this cyclonic circulation apparently interacted with the Himalaya  
132 foothills, which provided orographic lifting and further enhanced rainfall in Uttarakhand  
133 and adjoining regions (Joseph et al. 2014). During the post-storm period (Figures 1e and  
134 f), the upper-level trough weakened and the lower-level cyclonic circulation over the  
135 Indian peninsula dissipated.

136         The aforementioned analyses show that the June 2013 extreme precipitation event  
137 was likely caused by several factors acting collaboratively: (a) deepening of the upper-  
138 level trough leading to increased baroclinicity, cold air intrusion aloft, and enhanced  
139 instability with warm and moist air beneath, (b) strong monsoon trough in the lower  
140 troposphere merged with a BoB monsoon depression, and (c) interaction of the  
141 circulation with a steep topography on the southern side of the Himalayan ranges. These  
142 regional meteorological conditions are symptomatically similar to those in other extreme  
143 rainfall events in northern South Asia that involved upper-level synoptic waves (Wang et

144 al. 2011b; Rasmussen et al. 2014).

145

### 146 **3.2 Comparison with events of similar circulation settings**

147 To investigate whether or not this June 2013 event is singular or recurrent in the  
148 observational records and whether there is any systematic long-term change, we first  
149 identified cases since 1979 that featured the upper-level circulation setting similar to that  
150 of the June 2013 event. Since the midlatitude influence played a certain role (Joseph et al.  
151 2014) and such an influence has appeared to intensify (Wang et al. 2011a), we designed  
152 two selection criteria for the depiction of upper tropospheric circulations:

153 (1) For pattern recognition: The spatial correlation coefficient of 200 mb geopotential  
154 height anomalies in the region (20°N-60°N, 0°E-150°E) between the June 2013 storm  
155 period (13-17 June) and any given 5-day period is greater than 0.6 (i.e. with the p-  
156 value < 0.001).

157 (2) For trough intensity: The area-averaged geopotential height at the center of the upper-  
158 level trough (i.e., maximum vorticity in Fig. 1c to the northwest of Uttarakhand)  
159 averaged over any given 5-day period is within 60-140% of that in the 13-17 June  
160 2013 storm period.

161 These two criteria have to be met simultaneously to ensure proper identification of the  
162 upper-tropospheric circulation pattern and trough strength that both resemble those in the  
163 June 2013 event. Based on these criteria, only 5 cases were identified in the past 35 years  
164 (1979-2013): 22-26 June 2004, 12-16 June 2007, 28 June-2 July 2009, 28 June-2 July  
165 2010, and 28 June-2 July 2011. Apparently these cases only occurred in the last 10 years,  
166 implying that this type of meteorological setting (or midlatitude influence) conducive to

167 extreme rainfall is likely influenced by climate change.

168         In Figure 2 we compared the CMORPH precipitation (Figures 2a and b) and  
169 geopotential anomalies (Figures 2c-f) between the June 2013 event and the composite of  
170 all 5 cases identified previously. The accumulated precipitation in the composite cases  
171 does not show any significant amount in Uttarakhand (Figures 2b), even though the  
172 upper-level short-wave train (Figure 2d) shares a similar pattern with the 2013 event  
173 (Figure 2c). Why did these previous cases not produce rainfall as heavy as in June 2013  
174 in Uttarakhand? An examination of the 700 mb geopotential height structure gives a hint  
175 to this question: While the June 2013 event featured a strong monsoon trough (Figure 2e),  
176 the composite cases are characterized by a weak monsoon trough across the Indian  
177 subcontinent (Figure 2f). Altogether, these “similar but different” six cases reinforce the  
178 previous claim that the June 2013 event occurred due to the unusual coupling of the  
179 strong upper-level trough with a strong monsoon trough, and that these two anomalous  
180 circulations at different levels do not always synchronize.

181         Figure 3a displays the time series of June precipitation averaged over Uttarakhand  
182 (delineated with a box in Figure 1a), superimposed with an one-sided 20-year running  
183 average (black line) and a linear trend after 1988 (red line). Apparently there has been an  
184 increasing trend of precipitation during recent decades (with slope of 0.11 mm/day/year  
185 at 99% statistical confidence). As a further examination, Figure 3b shows the spatial  
186 pattern of the linear trend in the June 200 mb geopotential since 1988, reflecting the  
187 maximum precipitation trend. Figure 3c shows the 200 mb geopotential anomalies during  
188 the June 2013 event. A low pressure system is revealed in both Figure 3b and 3c to the  
189 north of Pakistan, which facilitates upper-level cold air intrusion towards northern India



190 and western Nepal. This coincidence suggests that the upper-level short-wave train  
191 associated with the June 2013 event is embedded in a long-term change in upper  
192 tropospheric circulation structure. The coincidence also echoes the finding of Wang et al.  
193 (2011b), who analyzed the 2011 Pakistan flood in July and found that the post-1980 trend  
194 in the upper troposphere exhibited an amplified short-wave structure similar to that of the  
195 circulation anomalies during summer 2011. These observations are supportive of the  
196 emerging theory that the jet stream may have become increasingly “meandering”; this  
197 leads to an increase in extreme events worldwide (Francis and Vavrus 2012; Wang et al.  
198 2013; Screen and Simmonds 2014).

199

### 200 **3.3 Attribution of the climate trend**

201 The next important question concerns the forcing mechanism that acts to  
202 strengthen the upper-level stationary waves near northern India. Here we analyzed the  
203 trend of the ensemble-mean 200 mb geopotential heights simulated by ten CMIP5 models  
204 for the period 1980-2005, and compared the results between the natural and GHG forcing  
205 experiments. As shown in Figure 4a, the simulation driven by all (natural and  
206 anthropogenic) forcing sources produced the 200 mb geopotential trends that are in  
207 reasonable agreement with the observation: i.e. an amplified wave train with an  
208 anomalous low center over central Asia and two anomalous high pressure centers located  
209 to the east and west. This result lends confidence in CMIP5 models’ performance.  
210 However, Figure 4b shows that the simulation with only natural forcing produced a  
211 circulation structure that does not favor cold air intrusion over northern South Asia. In  
212 contrast, both GHG and aerosols forcing simulations (Figures 4c and 4d) produced the

213 200 mb geopotential trends that are in line with the observation with the deepened trough  
214 to the north of Uttarakhand. This suggests that the increased greenhouse gases and likely  
215 the increased aerosols collectively caused wave train pattern of the change in the upper-  
216 level tropospheric flows. This result corresponds to the previous finding that all 5  
217 previous cases having a similar upper-level circulation setting with the June 2013 event  
218 occurred only in the last decade. Using three CMIP5 models, Wang et al. (2013) have  
219 found that only the GHG forcing experiments produced the amplified short waves during  
220 summer. In addition to the change in dynamics, we plotted in Figure 5 the June surface  
221 (2-meter) temperature averaged over Uttarakhand superimposed with the post-1988 trend  
222 (red line). The surface temperature in Uttarakhand only shows a mild warming trend that  
223 did not pass the significance test ( $p > 0.1$ ). This means that the upper tropospheric  
224 cooling is relatively more important for the destabilization and associated precipitation  
225 increase as revealed in Figures 3 and 4.

226         When it comes to attribution analysis, the mere use of observational data and  
227 model free runs is not adequate to reach robust conclusions. As a complementary  
228 approach, sensitivity experiments with WRF were performed (experimental design is  
229 detailed in Section 2.2). Figures 6a-c show 5-day average precipitation during the storm  
230 event (13-17 June) from the CMORPH as well as the control and no-trend experiments,  
231 respectively. The control experiment (Figure 6b) produced rainfall in Uttarakhand that  
232 agrees reasonably with the observation, while the no-trend experiment (Figure 6c) grossly  
233 underestimated precipitation. Apparently, the removal of long-term trend in the WRF  
234 boundary conditions considerably reduced the total storm rainfall. The ratio between the  
235 no-trend and control experiments (Figure 6d) indicates a 60-90% reduction in rainfall

236 over Uttarakhand (boxed area), and such a reduction in rainfall amounts is considered  
237 attributable to the long-term climate change. As further attribution, Figure 6e shows the  
238 daily precipitation evolution averaged over Uttarakhand. While the control experiment  
239 produced a comparable amount of rainfall with the observation, albeit with a shifted  
240 timing (delay) by about one day, the no-trend experiment produced significantly reduced  
241 precipitation, i.e., less than 20% over the entire period of 13-17 June. This result  
242 illustrates that, although the rainfall event would still occur regardless of the climate trend  
243 or change, the post-1980 climate trend in the atmosphere has significantly aggravated the  
244 storm intensity.

245         The mechanism through which the climate trend has contributed to the severity of  
246 the June 2013 event is further illustrated through thermodynamic analysis. Figures 7a and  
247 b show the vertical profiles of WRF-simulated potential temperature lapse rate ( $d\Theta/dp$ )  
248 and relative humidity averaged over the Uttarakhand region during 13-17 June 2013. The  
249  $d\Theta/dp$  of no-trend experiment revealed a discernable stabilization in the 800-650 mb  
250 layer relative to the control experiment. The increase in stability in the no-trend  
251 experiment is compounded by the apparent drying below 700 mb amounting to ~10% in  
252 relative humidity (Figure 7b). Thus, the combination of stabilization and drying in the  
253 lower troposphere, in addition to the weakening of the upper-level trough and wave train,  
254 supports the substantial rainfall reduction simulated by the no-trend experiment due to  
255 reduced conditional instability.

256

#### 257 **4. Concluding remarks**

258         We explored the meteorological and climatic conditions accompanying the June

259 2013 rainstorm event in northern India and analyzed past cases that feature similar upper-  
260 level circulation settings. The June 2013 event appears to be collaboratively generated by  
261 three factors: (a) an upper-level short-wave train with a cyclonic circulation over northern  
262 India leading to cold air intrusion, (b) a strong monsoon trough supplying moist air  
263 towards the Himalayan foothills, and (c) orographic lifting. The upper-level cold air  
264 intrusion enhances instability and subsequently increases rainfall intensity in the region.  
265 Furthermore, climate diagnoses suggest that the formation of the distinct short-wave train  
266 is not sporadic, but rather is reinforced by the long-term change in the upper troposphere.  
267 Based on the CMIP5 historical experiments, the upper-level wave train pattern revealed  
268 in the post-1980 trends is attributed to the increases in greenhouse gases and  
269 anthropogenic aerosols. Sensitivity experiments with the WRF model further indicated  
270 that the removal of the post-1980 trends in the forcing data leads to substantially reduced  
271 (~80%) precipitation in the flood region for the 5-day storm period. This estimated  
272 rainfall reduction is attributed to two prime factors: (1) suppressed cyclonic circulation in  
273 the upper troposphere restoring stability and (2) reduced moisture in the middle to lower  
274 troposphere. These processes favor the persistent increase in June rainfall over northern  
275 India after the mid-1980s and arguably contribute to the record amount of rainfall  
276 received in June 2013.

277         The conclusions reached in this study have implications for future flood  
278 management, water planning, and extreme weather prediction in northern South Asia.  
279 This study showed that as a result of anthropogenic climate change, the circulation  
280 structure has been modified in such a way that significantly aggravates rainstorm  
281 occurrences in northern South Asia, hence increasing the severity of floods. Also, the

282 occurrence of this June 2013 event during pre-monsoon season in northern South Asia,  
283 along with the circulation and precipitation trends in June, calls for prevention attention  
284 to increasingly frequent and strong rainstorms outside the core monsoon months (i.e.,  
285 July-August). Adaptation measures such as developing strategies and policies for flood  
286 management in the face of climate-related extreme events are urged. In addition, the  
287 amplified upper-level stationary waves and associated dynamics as revealed in this study  
288 will need to be represented accurately in the forecasting tools.

289

### 290 **Acknowledgements**

291 PRECL Precipitation data and NCEP Reanalysis data were provided by the  
292 NOAA/OAR/ESRL PSD, Boulder, Colorado, USA, from their Web site at  
293 <http://www.esrl.noaa.gov/psd/>. We would like to thank Henry Lin for his assistance. J.-H.  
294 Yoon is supported by the Office of Science of the U.S. Department of Energy as part of  
295 the Earth System Modeling program. PNNL is operated for the Department of Energy by  
296 Battelle Memorial Institute under Contract DEAC05-76RLO1830.

297

298	<b>List of Tables</b>
299	
300	Table 1: CMIP5 (the Coupled Model Intercomparison Project Phase 5) models used in the
301	attribution analysis.
302	
303	

304 **List of Figures**

305

306 Figure 1: Five-day mean wind (vectors) and relative vorticity (shadings) fields averaged  
307 over 8-12 June at (a) 200 mb and (b) 700 mb. for the pre-storm period. (c)-(d) Same as  
308 (a)-(b) but for the storm period of 13-17 June. (e)-(f) Same as (a)-(b) but for the post-  
309 storm period of 18-22 June. The Indian state of Uttarakhand is outlined (approximately)  
310 by the red box.

311

312 Figure 2: CMORPH precipitation averaged for (a) the storm event of 13-17 June 2013  
313 and (b) the composite of five past events with similar circulation settings (see text). (c)-  
314 (d) Similar to (a)-(b) but for the 200 mb geopotential anomalies (HGT), with the long-  
315 term mean removed. (e)-(f) Same as (c)-(d) but for the 700 mb geopotential anomalies.

316

317 Figure 3: (a) Time series of June precipitation averaged over the Uttarakhand region (red  
318 box in Figure 1) superimposed with a 20-year running mean (black line) and a linear  
319 trend after 1988 (red line). The 2013 amount is highlighted in red, indicating its record  
320 status. (b) The spatial pattern of the post-1988 linear trend (slope) in the 200 mb  
321 geopotential height(HGT); unit is meter per 25 years. Stippling indicates regions  
322 exceeding 90% statistical confidence. (c) The 5-day mean 200 mb geopotential height  
323 anomalies of 13-17 June 2013.

324

325 Figure 4: The 1980-2005 linear trend in the 200 mb geopotential height (HGT) simulated  
326 by (a) the all forcing, (b) the natural forcing, (c) the GHG forcing, and (d) the aerosols  
327 forcing experiments of 10 CMIP5 models. The unit is meter of total  
328 change over the 1980-2005 period. Stippling indicates regions exceeding 90% statistical  
329 confidence.

330

331 Figure 5: Time series of June surface temperature (2 meter) averaged over the  
332 Uttarakhand region (red box in Figure 1), superimposed with the post-1988 linear trend  
333 (red line).

334

335 Figure 6: Daily precipitation averaged for 13-17 June 2013 from (a) CMORPH, (b) the  
336 WRF control experiment, and (c) the no-trend experiment. (d) Percentage of precipitation  
337 reduction between the no-trend and control experiments; only the reduction in the no-  
338 trend experiment is shown. (e) 3-hour precipitation derived from CMORPH (blue), the  
339 control (black) and no-trend (red) experiments in Uttarakhand (boxed area).

340

341 Figure 7: Vertical profiles of (a) potential temperature lapse rate and (b) relative humidity  
342 averaged in Uttarakhand from the control (black) and no-trend (red) experiments  
343 averaged for 13-17 June 2013.

344

345

346

347  
348

**Table 1. CMIP5 (the Coupled Model Intercomparison Project Phase 5) models used in the attribution analysis**

Acronym	Full name	Number of ensemble	Developers
CanESM	Canadian Centre for Climate modeling and Analysis The second Generation Earth System Model 2	5	Canadian Centre for Climate Modelling and Analysis
CCSM4	Community Climate System Model version 4	3	National Center for Atmospheric Research
CNRM-CM5	National Centre for Meteorological Research Coupled Model 5	6	Centre National de Recherches Meteorologiques /Centre Europeen de Recherche et Formation Avancees en Calcul Scientifique, France
GFDL-CM3	Geophysical Fluid Dynamics Laboratory Coupled Physical Model 3	3	NOAA, Geophysical Fluid Dynamics Laboratory
GFDL-ESM2	Geophysical Fluid Dynamics Laboratory Earth System Model 2	1	NOAA, Geophysical Fluid Dynamics Laboratory
CSIRO	Commonwealth Scientific and Industrial Research Organization	4	Commonwealth Scientific and Industrial Research Organization/Queensland Climate Change Centre of Excellence (CSIRO-QCCCE)
FGOALS	Flexible Global Ocean-Atmosphere-Land System	1	Institute of Atmospheric Physics, Chinese Academy of Sciences
GISS-E2	Goddard Institute for Space Studies Model E2	3	NASA, Goddard Institute for Space Studies
IPSL-CM5	Institute Pierre Simon Laplace Coupled Model 5	3	Institute Pierre-Simon Laplace
NorESM1	Norwegian Earth System Model 1	1	Norwegian Climate Centre (NCC)

349  
350



351

352

353

354

## REFERENCES

355 Chen, M., P. Xie, J. Janowiak, and P. Arkin, 2002: Global land precipitation: A 50-yr

356 monthly analysis based on gauge observations. *J. Hydrometeorol.*, **3**, 249-266.

357 Collins, W. D. and Coauthors, , 2006: The formulation and atmospheric simulation of the

358 Community Atmosphere Model version 3 (CAM3). *J. Clim.*, **19**, 2144-2161.

359 Dubey, C. S., D. P. Shukla, A. S. Ningreichon, and A. L. Usham, 2013: Orographic

360 control of the Kedarnath disaster. *Curr. Sci.*, **105**, 1474-1476.

361 Hong, C., H. Hsu, N. Lin, and H. Chiu, 2011: Roles of European blocking and tropical-

362 extratropical interaction in the 2010 Pakistan flooding. *Geophys. Res. Lett.*, **38**, L13806.

363 Houze, R. A., Jr., K. L. Rasmussen, S. Medina, S. R. Brodzik, and U. Romatschke, 2011:

364 Anomalous Atmospheric Events Leading to the Summer 2010 Floods in Pakistan. *Bull.*

365 *Am. Meteorol. Soc.*, **92**, 291-298.

366 Joseph, S. and Coauthors, , 2014: North Indian heavy rainfall event during June 2013:

367 diagnostics and extended range prediction. *Clim. Dyn.* , *10. 1007/s00382-014-2291-5*, **in**

368 **press**

369 Joyce, R., J. Janowiak, P. Arkin, and P. Xie, 2004: CMORPH: A method that produces

370 global precipitation estimates from passive microwave and infrared data at high spatial

371 and temporal resolution. *J. Hydrometeorol.*, **5**, 487-503.

372 Kalnay, E. and Coauthors, , 1996: The NCEP/NCAR 40-year reanalysis project. *Bull. Am.*

373 *Meteorol. Soc.*, **77**, 437-471.

374 Kanamitsu, M., W. Ebisuzaki, J. Woollen, S. Yang, J. Hnilo, M. Fiorino, and G. Potter,

375 2002: NCEP-DOE AMIP-II reanalysis (R-2). *Bull. Am. Meteorol. Soc.*, **83**, 1631-1643.

376 Lau, W. K. M., and K. Kim, 2012: The 2010 Pakistan Flood and Russian Heat Wave:  
377 Teleconnection of Hydrometeorological Extremes. *J. Hydrometeorol.*, **13**, 392-403.

378 Lin, Y., and B. A. Colle, 2011: A New Bulk Microphysical Scheme That Includes Riming  
379 Intensity and Temperature-Dependent Ice Characteristics. *Mon. Weather Rev.*, **139**, 1013-  
380 1035.

381 Martius, O. and Coauthors, , 2013: The role of upper-level dynamics and surface  
382 processes for the Pakistan flood of July 2010. *Q. J. R. Meteorol. Soc.*, **139**, 1780-1797.

383 Najar, N. and S. Masood, Sept. 8, 2014: India and Pakistan Strain as Flooding Kills  
384 Hundreds. *The New York Times*, **2014**,  
385 [http://www.nytimes.com/2014/09/09/world/asia/hundreds-dead-in-flooding-in-india-and-](http://www.nytimes.com/2014/09/09/world/asia/hundreds-dead-in-flooding-in-india-and-pakistan.html?_r=0)  
386 [pakistan.html?\\_r=0](http://www.nytimes.com/2014/09/09/world/asia/hundreds-dead-in-flooding-in-india-and-pakistan.html?_r=0).

387 Nakanishi, M., and H. Niino, 2006: An improved mellor-yamada level-3 model: Its  
388 numerical stability and application to a regional prediction of advection fog. *Bound. -*  
389 *Layer Meteorol.*, **119**, 397-407.

390 Rasmussen, K. L., A. J. Hill, V. E. Toma, M. D. Zuluaga, P. J. Webster, and R. A. Houze  
391 Jr, 2014: Multiscale analysis of three consecutive years of anomalous flooding in  
392 Pakistan. *Quarterly Journal of the Royal Meteorological Society*, DOI: **10.1002/qj.2433**

393 Singh, D. and Coauthors, , 2014: Severe precipitation in Northern India in June 2013:  
394 causes, historical context, and changes in probability. *Explaining Extreme Events of 2013*  
395 *From A Climate Perspective: Special Supplement to the Bulletin of the American*  
396 *Meteorological Society*, **95**, 58-61.

397 Taylor, K. E., R. J. Stouffer, and G. A. Meehl, 2012: An Overview of Cmp5 and the  
398 Experiment Design. *Bull. Am. Meteorol. Soc.*, **93**, 485-498.

399 Wang, S., R. E. Davies, R. R. Gillies, and J. Jin, 2011a: Changing Monsoon Extremes and  
400 Dynamics: Example in Pakistan. *NOAA NWS, Science & Technology Infusion Climate*  
401 *Bulletin*, J. Zhao and W. Higgins eds., 61-68.

402 Wang, S., R. E. Davies, and R. R. Gillies, 2013: Identification of extreme precipitation  
403 threat across midlatitude regions based on short-wave circulations. *Journal of*  
404 *Geophysical Research-Atmospheres*, **118**, 11059-11074.

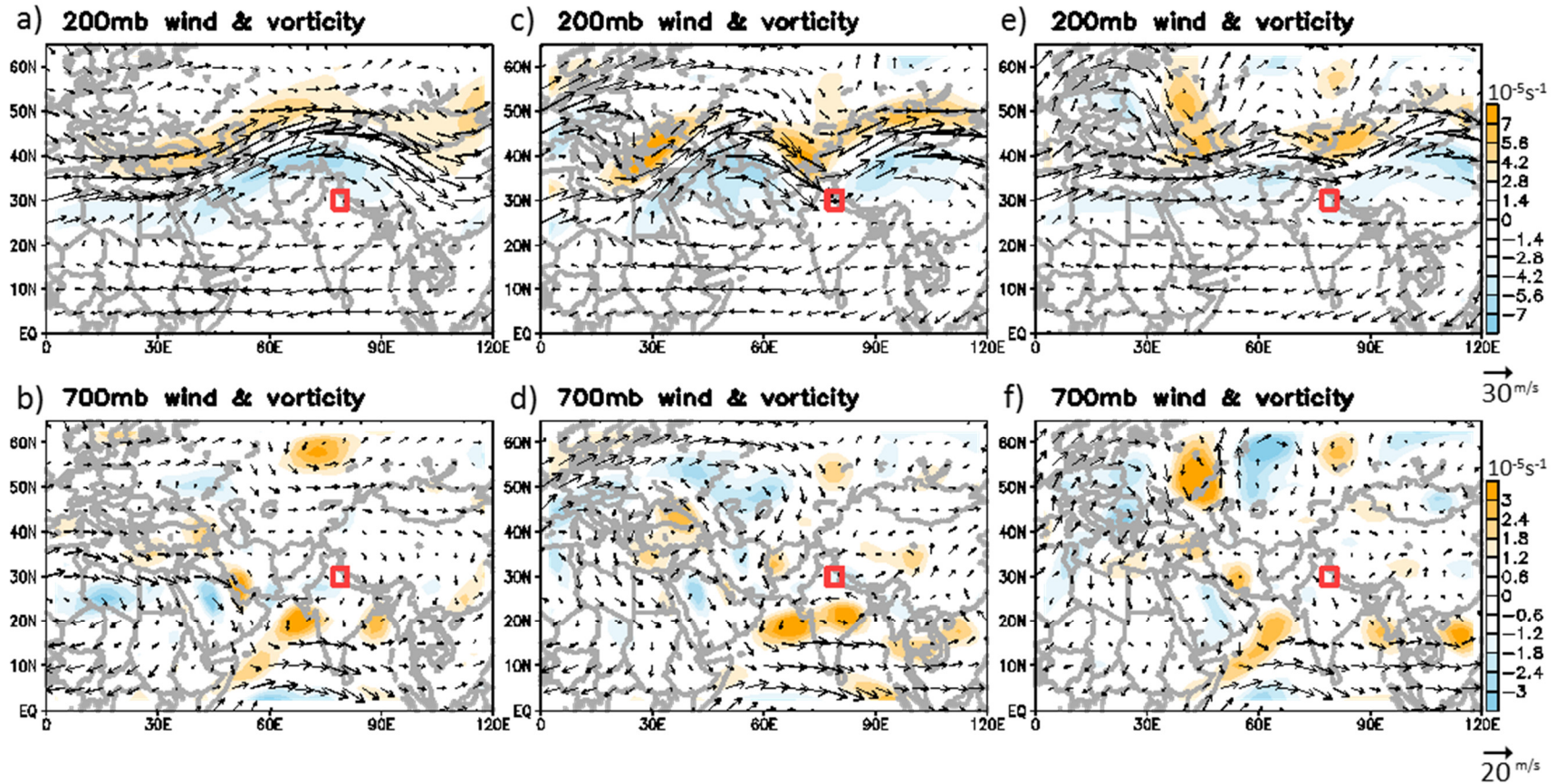
405 Wang, S., R. E. Davies, W. Huang, and R. R. Gillies, 2011b: Pakistan's two-stage  
406 monsoon and links with the recent climate change. *J. Geophys. Res. -Atmos.*, **116**,  
407 D16114.

408

Pre-storm

storm

post-storm



409

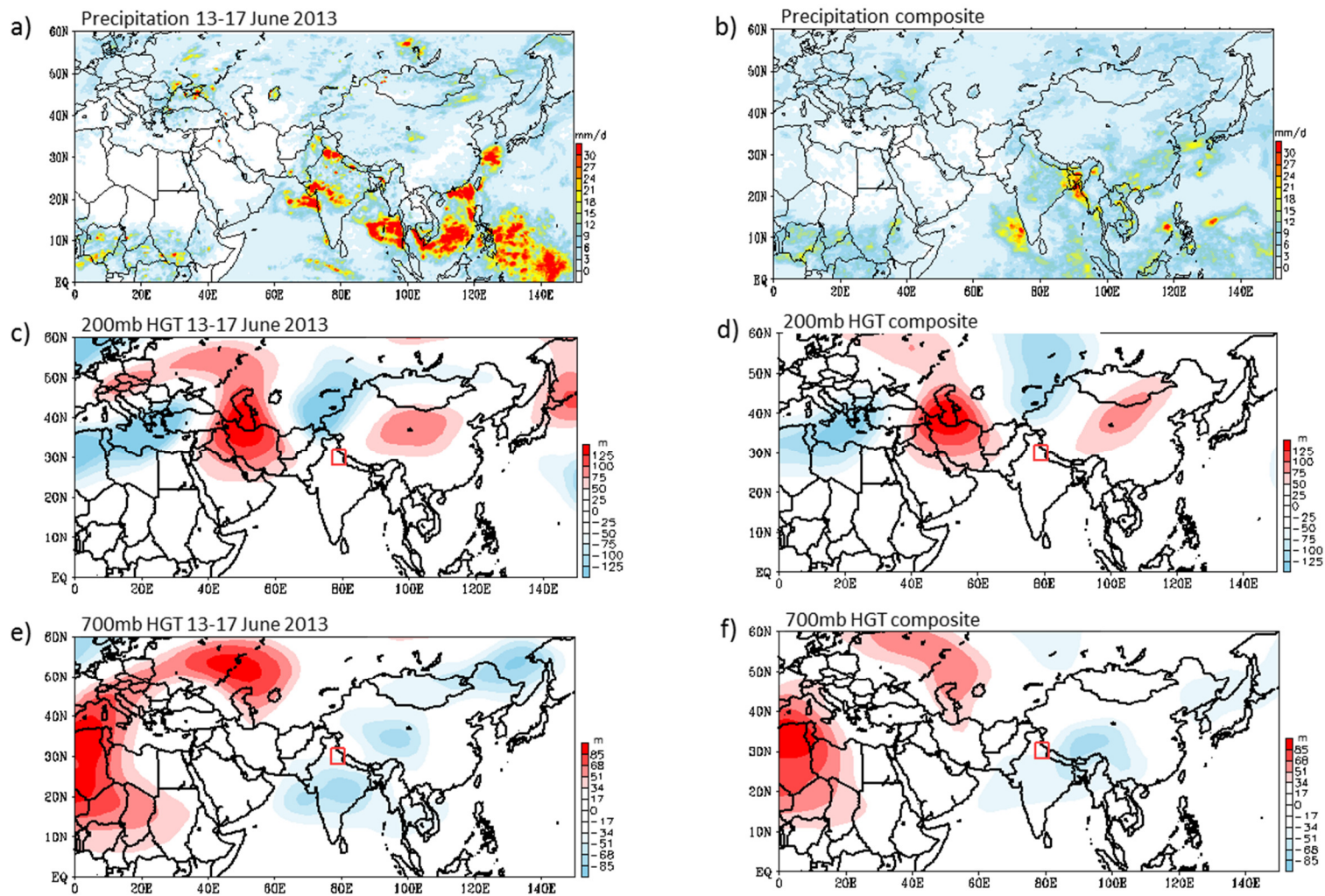
410

411

412

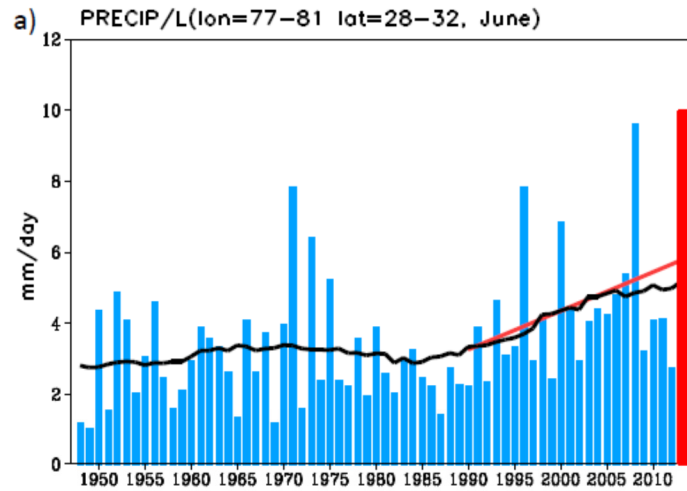
413

Figure 1: Five-day mean wind (vectors) and relative vorticity (shadings) fields averaged over 8-12 June at (a) 200 mb and (b) 700 mb. (c)-(d) Same as (a)-(b) but for the storm period of 13-17 June. (e)-(f) Same as (a)-(b) but for the post-storm period of 18-22 June. The Indian state of Uttarakhand is outlined (approximately) by the red box.

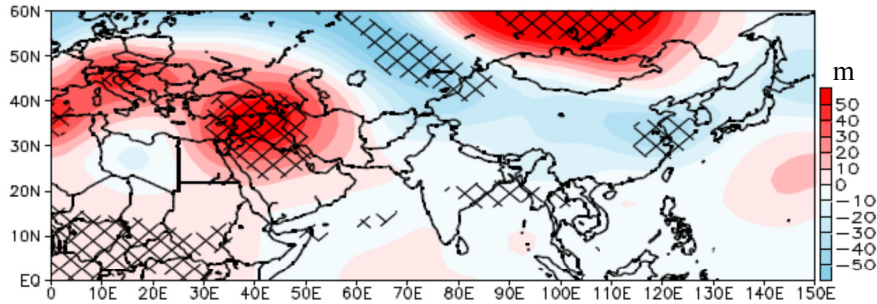


415  
416  
417  
418  
419

Figure 2: CMORPH precipitation averaged for (a) the storm event of 13-17 June 2013 and (b) the composite of five past events with similar circulation settings (see text). (c)-(d) Similar to (a)-(b) but for the 200 mb geopotential anomalies (HGT), with the long-term mean removed. (e)-(f) Same as (c)-(d) but for the 700 mb geopotential anomalies.



b) Trend in June 200mb height after 1988



c) Case 2013 HGT 200hPa

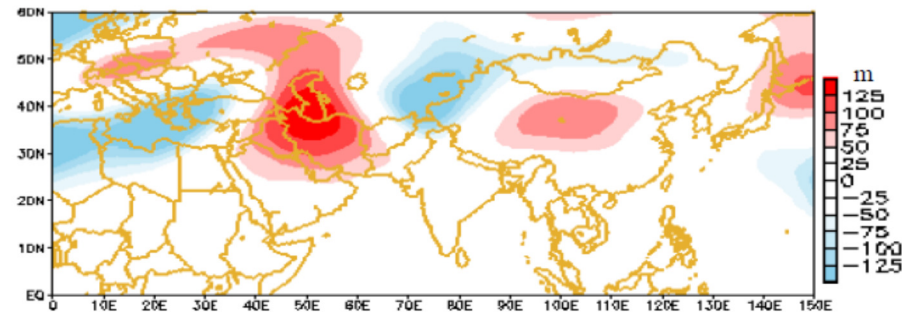
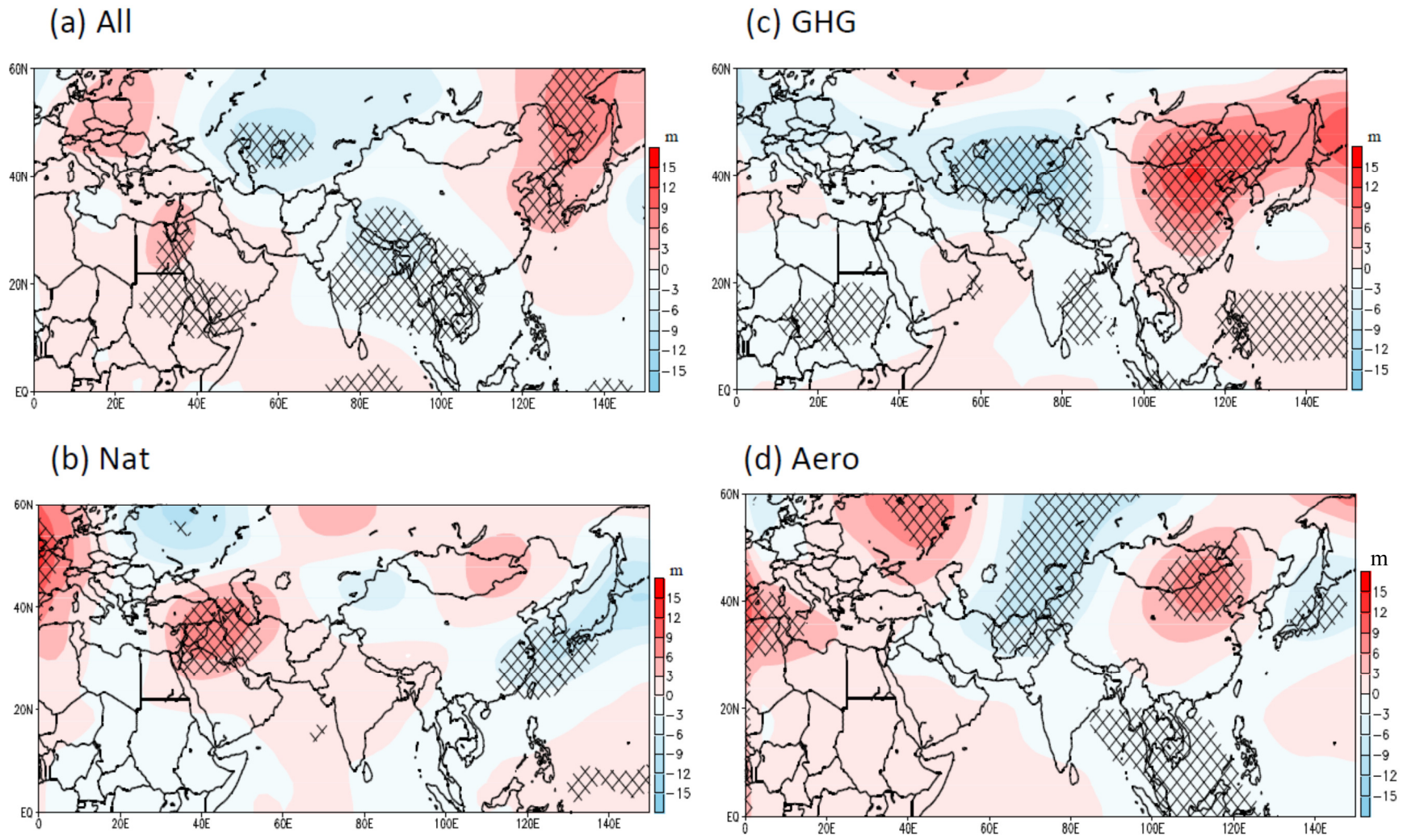


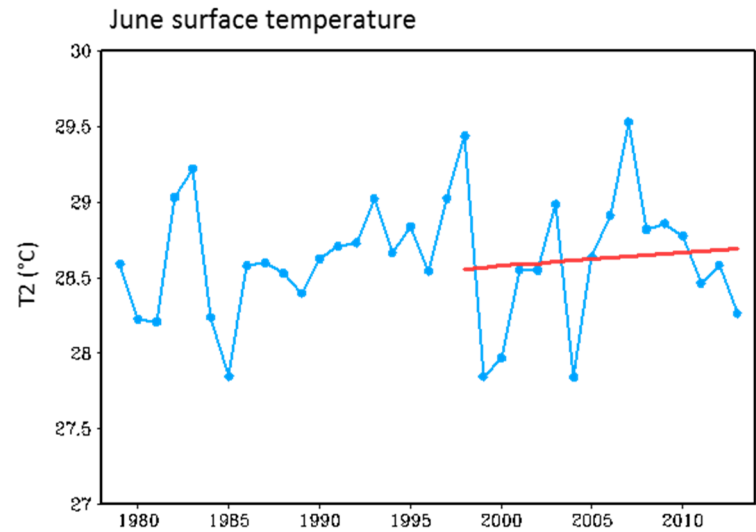
Figure 3: (a) Time series of June precipitation averaged over the Uttarakhand region (red box in Figure 1) superimposed with a 20-year running mean (black line) and a linear trend after 1988 (red line). The 2013 amount is highlighted in red, indicating its record status. (b) The spatial pattern of the post-1988 linear trend (slope) in the 200 mb geopotential height (HGT); unit is meter per 25 years. Stippling indicates regions exceeding 90% statistical confidence. (c) The 5-day mean 200 mb geopotential height anomalies of 13-17 June 2013.



421

Figure 4: The 1980-2005 linear trend in the 200 mb geopotential height (HGT) simulated by (a) the all forcing, (b) the natural forcing, (c) the GHG forcing, and (d) the aerosols forcing experiments of 10 CMIP5 models. The unit is meter of total change over the 1980-2005 period. Stippling indicates regions exceeding 90% statistical confidence.

422



423 Figure 5: Time series of June surface temperature (2 meter) averaged over the Uttarakhand region (red box in Figure 1), superimposed  
424 with the post-1988 linear trend (red line).  
425



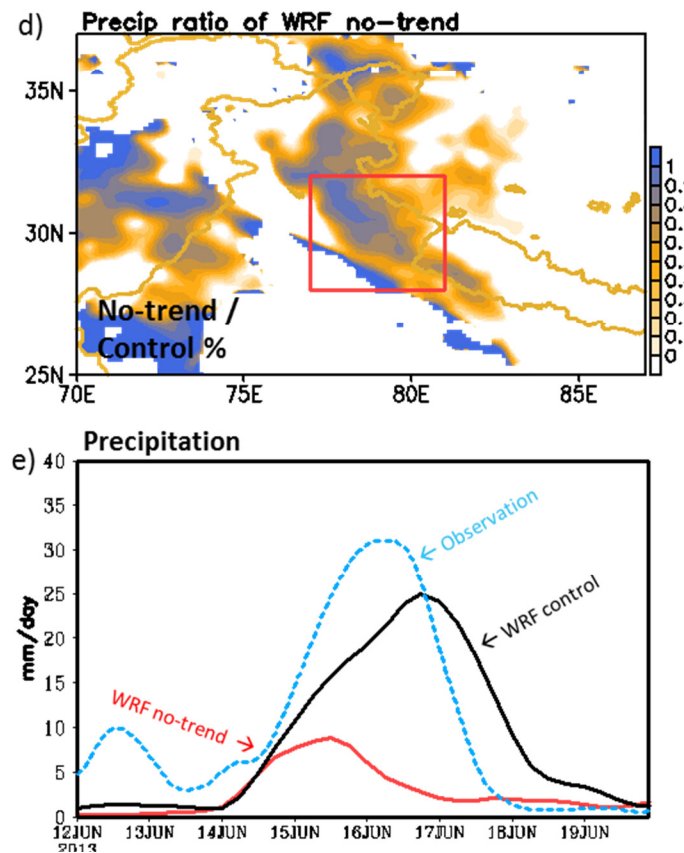
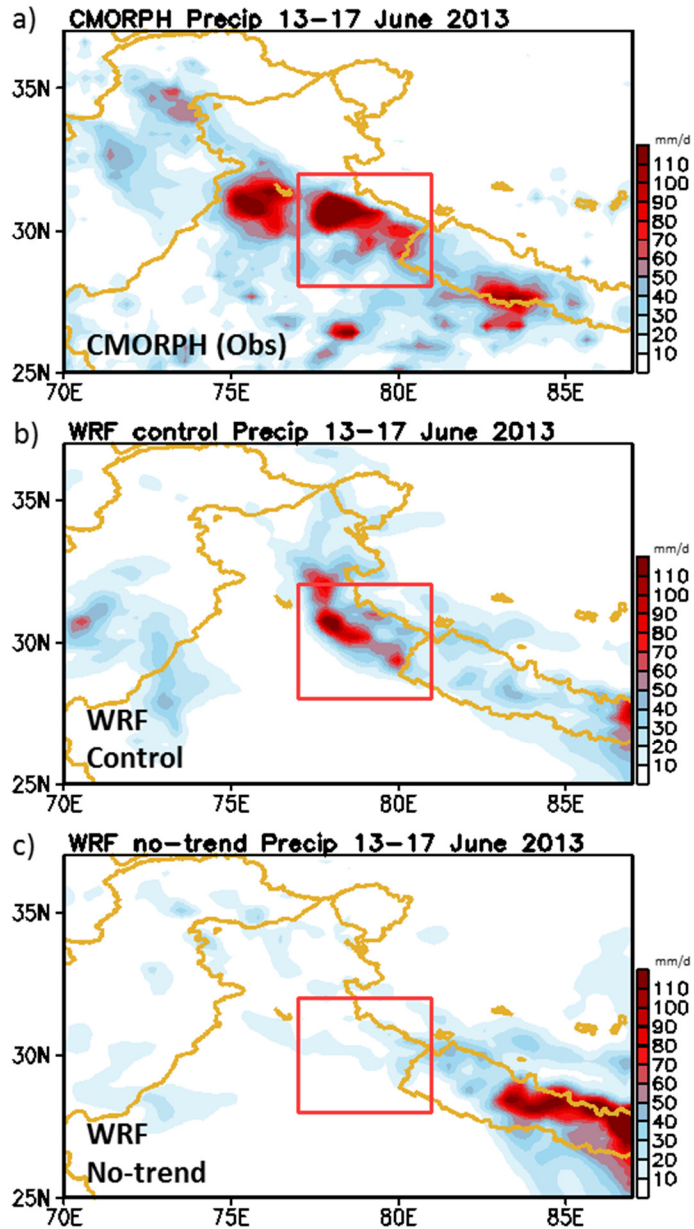
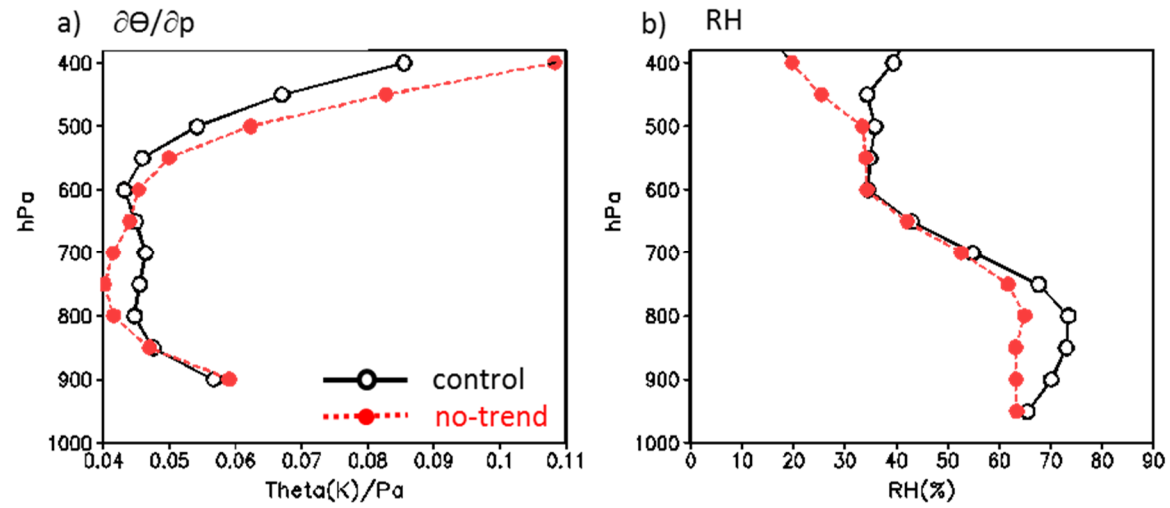


Figure 6: Daily precipitation averaged for 13-17 June 2013 from (a) CMORPH, (b) the WRF control experiment, and (c) the no-trend experiment. (d) Percentage of precipitation reduction between the no-trend and control experiments; only the reduction in the no-trend experiment is shown. (e) 3-hour precipitation derived from CMORPH (blue), the control (black) and no-trend (red) experiments in Uttarakhand (boxed area).

427



428

429

430 Figure 7: Vertical profiles of (a) potential temperature lapse rate and (b) relative humidity averaged in Uttarakhand from the control  
431 (black) and no-trend (red) experiments averaged for 13-17 June 2013.

432

433